ACS APPLIED ENERGY MATERIALS

www.acsaem.org Article

Reduction in Formation Temperature of Ta-Doped Lithium Lanthanum Zirconate by Application of Lux−Flood Basic Molten Salt Synthesis

J. Mark Weller and Candace K. Chan*

Cite This: *ACS Appl. Energy Mater.* 2020, 3, 6466−6475 Read Online

ACCESS | Metrics & More | Article Recommendations | Supporting Information

ABSTRACT: Garnets such as $Li_7La_3Zr_2O_{12}$ (LLZO) are important Li^+ conducting ceramics for potential use as solid electrolytes in solid-state batteries. However, LLZO is predominately prepared by using solid-state reaction methods, despite the high energy cost, multiple steps involved, and large particle sizes of the resultant material. Herein, molten salt synthesis (MSS) is applied to prepare Ta-doped LLZO ($Li_{6.4}La_3Zr_{1.4}Ta_{0.6}O_{12}$, LLZTO), demonstrating that control over the Lux−Flood basicity of the molten salt medium enables drastic reduction in the formation temperature relative to other synthetic methods. Each of the reaction media investigated, including eutectic LiCl−KCl, a mixture of LiCl−LiOH, and highly basic ternary mixtures of $LiNO_3$−LiOH−Li_2O_2, can be used to synthesize LLZTO under the appropriate experimental conditions. In the last case, garnet powders with predominately submicrometer particle sizes are obtained at temperatures as low as 550 °C. Sintered LLZTO pellets with high room temperature ionic conductivity can be obtained by using powders from each MSS method. LLZTO powders synthesized from the highly basic melts show good densification due to the small particle sizes (0.2−1 μm) and exhibit total ionic conductivity as high as 0.61 mS cm^{-1}. The results show that molten salt synthesis in media with high Lux−Flood basicity is an attractive low-temperature synthetic approach to achieving highly conducting garnet electrolytes.

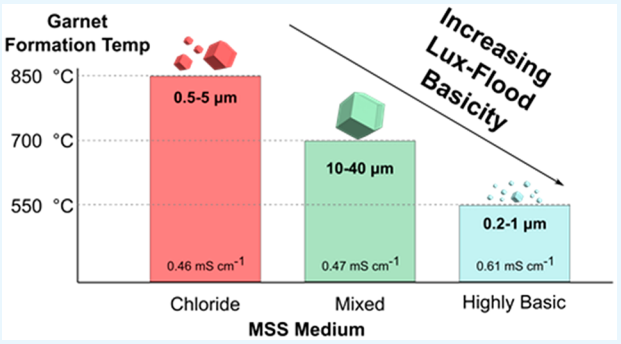

KEYWORDS: *LLZO, molten salt synthesis, garnet, solid electrolyte, solid-state lithium battery, sintering*

1. INTRODUCTION

Solid electrolytes are a critical technology to enable Li metal anodes for future solid-state lithium batteries (SSLBs).[1−3] Lithium-ion conducting garnets, particularly the family of doped lithium lanthanum zirconates ($Li_7La_3Zr_2O_{12}$, LLZO), offer a combination of high ionic conductivity, chemical and electrochemical stability against metallic lithium, low toxicity, and other beneficial properties.[1,2,4,5] LLZO is most commonly synthesized via solid-state reaction (SSR),[6] which requires high synthesis temperatures and often repeated grinding/milling and calcination operations to obtain phase-pure material.[7] Furthermore, since LLZO is polymorphic, the highly conducting cubic phase[2] must be stabilized by using dopants (such as Al,[8] Ga,[9] or Ta[10,11]) to prevent formation of the thermodynamically favorable but poorly conducting tetragonal[2,12] phase. Despite the simplicity of SSR and its use of relatively inexpensive, typically oxide reagents, the costs of synthesis coming from the high temperatures (>900 °C) and long reaction times (often >8 h, as high as 24 h) can be substantial. The resultant material also tends to exhibit irregular morphology and large particle size, necessitating additional milling steps prior to densification to increase its sinterability. Additionally, fine particles are highly desirable[13,14] for formation of LLZO thin films when using approaches such as tape casting,[15,16] requiring extensive high-energy milling if using LLZO synthesized via SSR. Therefore, a method that can produce small (e.g., submicrometer) LLZO powders at a reasonable scale would be highly advantageous to reduce processing steps and eliminate other unintended consequences, such as ball-milling-induced amorphization[17] of the milled material.

The desire to obtain submicrometer to nanosized LLZO at lower synthesis temperatures has motivated us and others to prepare LLZO via methods alternative to SSR such as sol−gel,[18,19] polymer combustion,[20−26] coprecipitation,[10,27−29] and electrospinning.[30−32] In general, these methods require more expensive reagents, still use relatively high processing temper-

Received: March 31, 2020
Accepted: June 3, 2020
Published: June 3, 2020

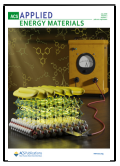

https://dx.doi.org/10.1021/acsaem.0c00716
ACS Appl. Energy Mater. 2020, 3, 6466−6475

atures to obtain crystalline LLZO (generally 700 °C or more), and only allow for relatively low throughput of material.

Molten salt synthesis (MSS) is a versatile synthetic strategy for the preparation of oxides at temperatures and times lower than those required for SSR, with better control over particle size and morphology.[33,34] In MSS, a salt or salt mixture is heated above its melting point and used as a solvent to dissolve precursor reagents, which subsequently form the desired product via dissolution, nucleation/precipitation, and crystal growth.[33] We recently demonstrated that submicrometer LLZO particles can be prepared with MSS by using a LiCl−KCl eutectic mixture as solvent, although a reaction temperature of 900 °C was still required to obtain phase-pure LLZO.[35] One strategy for reducing the reaction temperature for oxide formation in MSS is by utilizing more basic melt components such as oxobases (e.g., $LiNO_3$ and LiOH).[33] Acidity and basicity for oxides are described in the Lux−Flood acid−base theory, wherein a base is an O^{2-} donor (e.g., $Li_2O \rightarrow 2Li^+ + O^{2-}$) and an acid is an O^{2-} acceptor (e.g., $SiO_2 + O^{2-} \rightarrow SiO_3^{2-}$).[36,37] A basicity index analogous to pH can be defined in this way based on the concentration of O^{2-} in the melt ($pO^{2-} = -\log([O^{2-}])$, related to the concentration and nature of bases used. The ability of more basic molten salts to liberate more O^{2-} at lower temperatures results in a shift in acid−base equilibrium, which favors the precipitation of oxide phases,[33] thereby providing a stronger thermodynamic driving force for oxide formation. For example, $Li_4Ti_5O_{12}$ (LTO) can be synthesized in molten LiCl−KCl at 800 °C,[38] whereas utilization of a Lux−Flood basic molten salt medium based on the ternary $LiNO_3$−LiOH−Li_2O_2 system enables formation of LTO at temperatures as low as 300 °C.[39] For comparison, LTO synthesized via SSR requires temperatures between 800 and 1000 °C.[39] Other examples of MSS of oxides in the literature have noted a similar effect, wherein increased basicity of the melt components (e.g., use of nitrite over nitrate salts) can confer a greater decrease in formation temperature of a given oxide.[40]

Herein, this effect is leveraged for preparation of Ta-doped LLZO (LLZTO, nominal composition $Li_{6.4}La_3Zr_{1.4}Ta_{0.6}O_{12}$), which is known to possess exceptionally high conductivity among Li garnets.[41] Doping of LLZO with Ta is advantageous as Ta resides on the Zr sites in the garnet structure and therefore does not disrupt or impede Li diffusion on the Li sublattice like other dopants such as Al or Ga.[42] Additionally, Ta doping provides better electrochemical stability compared to other Zr-site dopants such as Nb.[43] For synthesis of LLZTO, several molten salt media of increasing basicity were employed by successively increasing the proportion of oxobases in the melt, beginning with eutectic LiCl−KCl (from now on termed the "chloride" melt), progressing to a mixture of LiCl and LiOH (which we call the "mixed" melt), and finally a ternary mixture of oxobases consisting of $LiNO_3$−Li_2O_2−LiOH (which we call the "highly basic" or HB melt). We show that the formation temperature of LLZTO can be successively reduced by increasing the basicity of the melt, and the morphology and particle size of the resultant material can also be controlled by the nature of the salt medium utilized.

2. EXPERIMENTAL SECTION

2a. Materials and Reagents. All reagents used were of ACS grade or higher unless otherwise noted and used as-received. Lithium nitrate ($LiNO_3$, anhydrous), lithium hydroxide (LiOH, anhydrous), zirconium oxychloride octahydrate ($ZrOCl_2{\cdot}8H_2O$), tantalum oxide (Ta_2O_5), lanthanum hydroxide ($La(OH)_3$), and lanthanum nitrate hexahydrate ($La(NO_3)_3{\cdot}6H_2O$) were obtained from Alfa Aesar. Zirconium oxynitrate hydrate ($ZrO(NO_3)_2{\cdot}xH_2O$) was obtained from Sigma-Aldrich. Lithium peroxide (Li_2O_2, technical grade, 95%) was obtained from Acros Organics. Isopropanol (ACS grade) and methanol (HPLC grade) were obtained from BDH Chemicals.

2b. Molten Salt Synthesis of LLZTO in Eutectic LiCl−KCl (Chloride MSS Method). The flux forming salts (LiCl and KCl in a 0.59:0.41 molar ratio) were mixed with the LLZTO reagents ($LiNO_3$, $La(NO_3)_3{\cdot}6H_2O$, $ZrOCl_2{\cdot}8H_2O$, and Ta_2O_5) by using a mortar and pestle in a mass ratio of 3:1. The Li:La:Zr:Ta molar ratio used was 9.6:3:1.4:0.6 (50% excess Li) for a targeted nominal composition $Li_{6.4}La_3Zr_{1.4}Ta_{0.6}O_{12}$. The mixture (typically ∼40 g total) was placed in an alumina crucible (Coorstek high alumina, 250 mL volume) and heated at a rate of 5 °C min^{-1} to the reaction temperature in a muffle furnace (Carbolite ELF 11 type). The synthesis was performed in air. The mixture was held for 4 h at 850 or 900 °C. It was found that Ta-doped LLZO forms at a somewhat lower temperature than undoped, Al-doped, and Ga-doped LLZO reported in our previous work.[35]

2c. Molten Salt Synthesis of LLZTO in LiCl−LiOH (Mixed-MSS Method). The flux forming salts (LiCl and LiOH, mass ratio 1:1) were mixed with the same reagents at a mass ratio of 2:1 (total mass ∼30 g) as described in the chloride MSS method (with the exception that for these experiments, $ZrO(NO_3)_2$ was used instead of $ZrOCl_2$), heated at a rate of 5 °C min^{-1} in alumina crucibles (Coorstek, high alumina, 100 mL), and held at 550−900 °C for various times between 1 and 8 h in a muffle furnace (Thermo Scientific LindBerg Blu M muffle furnace or Carbolite ELF 11 type muffle furnace). The synthesis was performed in air. The ratio of flux salts to reagents was 2:1 by mass.

2d. Molten Salt Synthesis of LLZTO in $LiNO_3$−LiOH−Li_2O_2 (HB- and mHB-MSS Method). In general, the flux forming salts ($LiNO_3$, LiOH, and Li_2O_2) were coarsely mixed and heated at a rate of 5 °C min^{-1} in alumina crucibles (Coorstek, high alumina, 100 mL) to the reaction temperature. Reactions were performed in a small muffle furnace (MTI Corporation KSL-1100X). For the highly basic method (HB-MSS), the molar ratio of $LiNO_3$:LiOH:Li_2O_2 was 1:2:2 while the modified highly basic method (mHB-MSS) adopted a molar ratio of 1.1:3.2:1 to afford a less viscous molten reaction medium. It should be noted that since $LiNO_3$ decomposes above 600 °C,[44] the reaction temperature used should be below 600 °C. Most reactions were performed at 550 °C. Once the desired hold temperature was reached, the furnace door was opened and the mixture was briefly (∼15 s) stirred by manually agitating the crucible with tongs to ensure homogeneity of the molten salts. This process must be performed with appropriate PPE (lab coat, goggles, and heat resistant gloves) to protect from heat from the furnace and against any accidental splashing of salts; it is also recommended that the furnace be placed inside a fume hood.

Reagents ($ZrO(NO_3)_2$ was used for initial experiments while $ZrOCl_2$ was used for the majority of experiments; no noticeable difference was observed between the two Zr sources) were premixed by using a mortar and pestle with some methanol followed by drying at 120 °C in air until all methanol was removed to produce a uniform reagent mixture. Subsequently, the premixed, dried, stoichiometric reagents were slowly added to the molten HB or mHB flux, followed by stirring as above for roughly 15 s to ensure homogeneity of the reagents. After adding reagents, we placed the crucible back inside the furnace to maintain temperature. Then, the aforementioned stirring procedure was repeated after 5 min inside the furnace and the reaction was allowed to proceed for the remainder of the hold time. *It should be noted that salts that contain water or may evolve gases (such as from the decomposition of nitrates) should be added to molten salts slowly and with extreme care to prevent splashing of hot molten salts.* The mass ratio of flux salts to reagents was 5:1 for the HB-MSS method and 1.7:1 for the mHB-MSS method. Generally, reaction sizes of ∼30 g were used. The mixture was held for various times (between 0−4 h for HB-MSS and 4−24 h for mHB-MSS) at the desired temperature. The synthesis was performed in air.

https://dx.doi.org/10.1021/acsaem.0c00716
ACS Appl. Energy Mater. 2020, 3, 6466−6475

2e. Postsynthesis Processing. After each of the above MSS reactions, the crucibles were cooled naturally to room temperature in the furnace. Then, ultrapure water (>18 Mohm cm) was added to the cooled crucibles, and the suspension was ultrasonicated by using an immersion probe (Cole-Parmer 500 W ultrasonic processor) to rapidly dissolve the salts and generate a slurry containing the LLZO powders. Subsequently, the slurry was vacuum filtered by using poly(vinylidene fluoride) membranes (0.22 μm pore size, DuraPore, EMD) and washed thoroughly and repeatedly with water followed by a small amount of methanol to facilitate faster drying. In general, 300 mL of water was used for the reaction sizes above, followed by 50 mL of methanol. Finally, the filter membranes along with the wet powder cakes were placed in an oven at >100 °C and dried in air. After drying, the LLZO powders were removed from the filter membranes and lightly ground with a mortar and pestle. Scheme 1 summarizes the general synthetic approach for each of the three categories of MSS used herein.

Scheme 1. General Synthetic Process for Molten Salt Synthesis (MSS) of LLZO Garnet Using the Chloride-MSS (LiCl–KCl), Mixed-MSS (LiCl–LiOH), and HB-MSS ($LiNO_3$–Li_2O_2–LiOH) Salt Media Used in This Work[a]

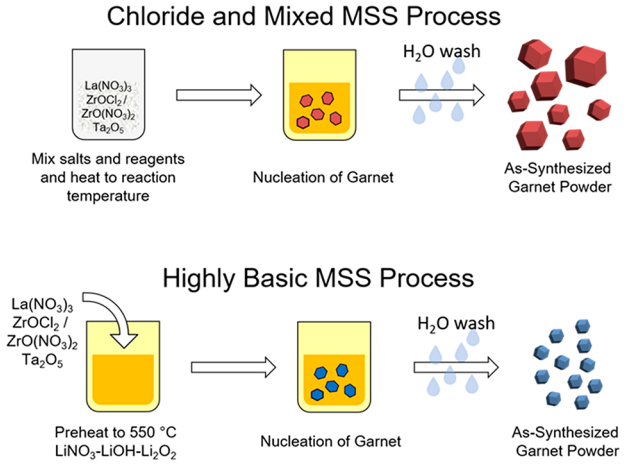

[a]For the chloride- and mixed-MSS, the salts and reagents are mixed together before heat treatment followed by a standard temperature ramp in the furnace. For the HB-MSS, the lower synthesis temperature allows a "reagent feeding" method to be employed, where the salts are preheated to the reaction temperature and the reagents are subsequently added. This approach initiates the reaction at the desired reaction temperature, rather than relying on a slow furnace ramp to the desired reaction temperature.

2f. Solid-State Reaction of LLZTO for Use as Mother Powder. For use as mother powder for sintering, LLZTO of the same composition as that prepared by using the MSS methods was synthesized via the solid-state reaction (SSR) method. Stoichiometric $La(OH)_3$, ZrO_2, and Ta_2O_5 with 20% excess Li_2CO_3 (based on the composition $Li_{6.4}La_3Zr_{1.4}Ta_{0.6}O_{12}$) were used as reagents. The reagents were ball-milled (MSE Supplies benchtop planetary ball-mill, Tucson, AZ) in an equivalent mass of 2-propanol by using a planetary ball mill. Zirconia jars and milling media were used, and the mill was operated at 700 rpm for 4 h. Subsequently, the milled reagents were collected, and the 2-propanol was evaporated in a fume hood. The powder was transferred to a MgO crucible (Tateho Ozark Technical Ceramics round tray with flanged MgO lid, part # SR3005 for crucible and SF300 for the lid) and calcined once at 1000 °C for 8 h. The synthesis was performed in air. After calcination, the powder was lightly ground with an agate mortar and pestle to deagglomerate before use.

2g. Preparation of Ceramic Pellets. LLZTO pellets were consolidated from powders via uniaxial cold-pressing (SpecAc Atlas 15T Manual Hydraulic Press) using a 7 mm stainless steel die. The LLZTO from the chloride, mixed, and mHB MSS were ball-milled (SPEX 8000M) before pressing and sintering to attempt to eliminate any effect of particle size on sinterability. The HB–MSS powders and some mHB–MSS powders were densified without ball-milling. Pellets were uniaxially pressed by using 125 MPa pressure for 5 min at room temperature. Additionally, 5% LiOH was added to the mixed–MSS LLZTO powder before ball-milling due to its low sinterability.

Pressed green pellets were sintered at 1200 °C for between 2 and 4 h. One HB–MSS pellet was sintered at 1300 °C for 3 h. Sintering was performed in a Thermo Scientific Lindberg Blue M 1700 °C box furnace. For sintering, pellets were placed on a small bed of mother powder (synthesized via conventional solid-state reaction; see section 2f) atop a porous MgO substrate, as MgO is known[45,46] to be more inert to LLZO and Li_2O than most other crucible materials besides Pt. All pellets were sintered in MgO crucibles in air (Tateho Ozark Technical Ceramics). For initial sintering of the HB–MSS LLZTO, a large excess of mother powder (4:1 mother powder mass to pellet mass) was also placed below the porous MgO substrate and within the crucible (part # SC15020 for the crucible and part# SF150 for the lid) to maintain a high Li_2O vapor pressure, which has been shown[46] to be crucial for achieving high pellet densities. During experimentation and optimization a new mother powder composition was used wherein a mixture of mother powder and Li_2O_2 was employed (6:3:1 mass ratio of mother powder:pellet:Li_2O_2) placed below the porous MgO substrate inside of the MgO crucible to provide a Li_2O-rich vapor phase. Minimal mother powder was still used underneath pellets to prevent stiction. This new mother powder composition was used for sintering the chloride-MSS, mixed-MSS, and mHB-MSS LLZTO powders. The use of a mixture of LLZTO and Li_2O_2 was also investigated in our previous work[26] and allows for comparable sintering while minimizing wasted LLZTO mother powder. All crucibles were covered with a MgO lid (Tateho Ozark Technical Ceramics) during sintering using the same arrangement as that used in our previous work.[26] For these sintering experiments, the smallest crucibles possible were used to minimize evaporation of Li (in our case, generally 1 in. diameter and 0.5 in. tall crucibles, Tateho Ozark part #'s SR1005 and SF100). Small MgO crucibles were contained within larger Al_2O_3 crucibles for sintering to contain Li vapor and prevent interaction with the furnace heating elements. We would like to note that excess Li vapor can cause substantial damage to furnace heating elements over time if not contained adequately. The density of the as-sintered pellets was calculated from the sample geometry (measured with a micrometer) and mass and compared to the theoretical density of $Li_{6.4}La_3Zr_{1.4}Ta_{0.6}O_{12}$ (5.5 g cm^{-3}).[47]

2h. Materials Characterization. X-ray diffraction (XRD) was performed by using either a Siemens D-5000 or a Bruker D-8 powder diffractometer with Cu Kα radiation for crystalline phase identification. The reference pattern for c-LLZO ($Ia\bar{3}d$) was generated according to the structure reported by Logeat et al.[11] The sample morphology was examined by using a FEI XL30 scanning electron microscope (SEM) equipped with an EDAX system for energy dispersive spectroscopy (EDS). To minimize charging, a carbon film was deposited on the samples before imaging using a thermal evaporator type carbon coater.

Transmission electron microscopy (TEM) was performed by using an aberration-corrected (CEOS image corrector) FEI Titan Environmental TEM operated at 300 kV. For high-resolution aberration-corrected TEM imaging, aberrations were corrected to yield an imaging resolution better than 1 Å, and negative spherical aberration imaging (Cs ~ −13 μm) was employed to yield bright contrast at the positions of atom columns. Electron diffraction (ED) patterns were obtained by using a third condenser lens to allow formation of a submicrometer diameter parallel beam rather than using a selected area aperture. To prepare TEM samples, the LLZO powder was ultrasonically suspended in HPLC-grade methanol. A holey carbon TEM grid (Pacific Grid Tech) was then briefly immersed into the aforementioned suspension. Finally, the grid was dried at elevated temperature (e.g., 100 °C) in air to fully remove methanol.

https://dx.doi.org/10.1021/acsaem.0c00716
ACS Appl. Energy Mater. 2020, 3, 6466–6475

Electrochemical impedance spectroscopy (EIS) was performed by using a BioLogic SP-200 potentiostat (maximum frequency 7 MHz, minimum frequency 1 kHz−1 Hz depending on measurement). The ionic conductivity of sintered pellets was measured by using either graphite[48] blocking electrodes or Sn−Li alloy[49] nonblocking electrodes. The temperature dependence of ionic conductivity was assessed between 273 and 353 K for select samples using Sn−Li alloy electrodes. Detailed descriptions of the procedures used for electrochemical measurements are in the Supporting Information.

3. RESULTS AND DISCUSSION

3a. Synthesis of $Li_{6.4}La_3Zr_{1.4}Ta_{0.6}O_{12}$ in Various Molten Salt Media. To understand the formation process of LLZTO in the various MSS reactions, a series of syntheses were performed at different temperatures. In all cases, phase-pure LLZTO can be prepared under the appropriate experimental conditions (Figure 1). Initial attempts at forming cubic Al-doped LLZO and Ga-doped LLZO in the basic media were unsuccessful (i.e., resulting in tetragonal LLZO), likely due to the poor solubility of Al_2O_3 or Ga_2O_3. Therefore, LLZTO was the focus of further study. In the case of MSS in the LiCl−KCl medium, the formation process of undoped LLZO was described previously, with lanthanum oxychloride (LaOCl) forming at 500 °C followed by formation of pyrochlore-type lanthanum zirconate ($La_2Zr_2O_7$, LZO) beginning at 600 °C and finally LLZO at 900 °C.[35] Interestingly, LLZTO with a Ta-doping level of 0.6 mol per formula unit (PFU) forms at only 850 °C (Figure S1), 50 °C lower than that needed to synthesize undoped LLZO in the same melt. This seems to indicate that Ta-doping results in a more energetically favorable phase than undoped LLZO, which is corroborated by calculations from Miara et al.,[50] wherein increasing the Ta content from 0 to 2 mol PFU results in a decrease of the decomposition energy, implying a more stable cubic garnet phase.

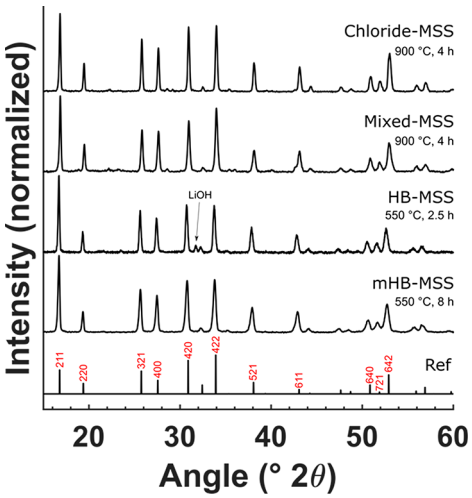

Figure 1. XRD patterns of LLZTO synthesized using molten salt synthesis (MSS) in the chloride (900 °C 4 h), mixed (900 °C, 4 h), HB (550 °C, 2.5 h), and modified HB (550 °C, 8 h) melts; reference pattern produced according to Logeat et al.[11] with major reflections labeled with (red) corresponding Miller indices. LiOH present in the HB−MSS sample is due to the large amount of salts used to form the melt and some residue after washing.

XRD patterns for LLZTO syntheses in the mixed and HB melts are shown in Figure S2. In both media, phase-pure garnet powders can be obtained under the appropriate experimental conditions. In the case of MSS in the mixed halide/hydroxide melt, similar to the pure chloride melt, LaOCl and LZO intermediates form before LLZO; the increased basicity of LiOH, however, allows formation of LLZTO at only 700 °C (Figure S2a). The morphology of these intermediates is the same as previously reported[35] and can be seen in Figure S3a.

On the other hand, LLZTO can form at much lower temperatures by using the highly basic, ternary salt medium. Because of the $LiNO_3$ present in this mixture, the maximum feasible reaction temperature is ∼600 °C, as $LiNO_3$ decomposes[44] above this temperature. One advantage of the low synthesis temperature in HB−MSS is the ability to add reagents ("reagent feeding") to the melted salts, essentially "starting" the reaction at the desired temperature rather than requiring a slow temperature ramp. This distinction is depicted in Scheme 1. However, the high viscosity of the pastelike mixture below 550 °C made uniform addition of reagents challenging. Nonetheless, synthesis at 450 °C was attempted, and $La(OH)_3$, $LiTaO_3$, and a small amount of LLZTO were observed in the XRD pattern of the products (Figure S2b). Curiously, no other intermediate Zr-containing phases such as $La_2Zr_2O_7$ or ZrO_2 were observed, which may indicate that Zr is sequestered in amorphous intermediates. The morphology of the intermediates from the HB synthesis at 450 °C is shown in Figure S3b.

Because of the lower viscosity of the melt at 550 °C, most experiments using HB-MSS were conducted at this temperature. A time-dependent study (Figure S2b) showed that, initially, $La(OH)_3$ is the main crystalline phase formed, but it eventually reacts and small amounts of $LiTaO_3$, La_2O_3, and LLZTO are formed after 1 h at 550 °C. Phase pure LLZTO is obtained by using reaction times of 2.5−4 h at 550 °C. Some reactions were performed at 550 °C for 4 h without either $LiNO_3$ or LiOH, and both resulted in incomplete formation of LLZTO (Figure S2b). On the basis of these results, we conclude that all three flux components are important to efficiently form LLZTO in the case of HB-MSS. There appears to be a synergistic effect of these three components that results in the effectiveness of the HB-MSS method, wherein the relatively low melting point of $LiNO_3$ (∼264 °C)[44] helps to reduce the melting point of the mixture, LiOH acts as an amphoteric solvent,[51] and Li_2O_2 acts as a base, liberating reactive oxygen species as it decomposes[52] starting around 250 °C, while also forming reactive Li_2O.

Representative scanning electron microscopy (SEM) images of LLZTO prepared from each method are shown in Figure 2a−c. The particle size range of the LLZTO powders synthesized in the halide melt (Figure 2a) corresponds well with that of undoped, Al-doped, and Ga-doped LLZO synthesized in the same melt previously by our group,[35] although the size distribution is slightly larger, possibly due to the energetic favorability of forming LLZTO compared to other forms of LLZO as discussed previously. In contrast, LLZTO synthesized in the mixed melt (Figure 2b) presents as substantially larger faceted particles with sizes ranging from 10 to 40 μm, implying that single crystal growth is favored. LLZTO synthesized in the highly basic medium (Figure 2c) generally has the smallest particle size, with the primary particle size ranging from 200 to 500 nm (though many individual nuclei are fused together) up to about 2 μm for a small number of particles. These results indicate a complex interrelationship between melt basicity and the solvent

https://dx.doi.org/10.1021/acsaem.0c00716
ACS Appl. Energy Mater. 2020, 3, 6466−6475

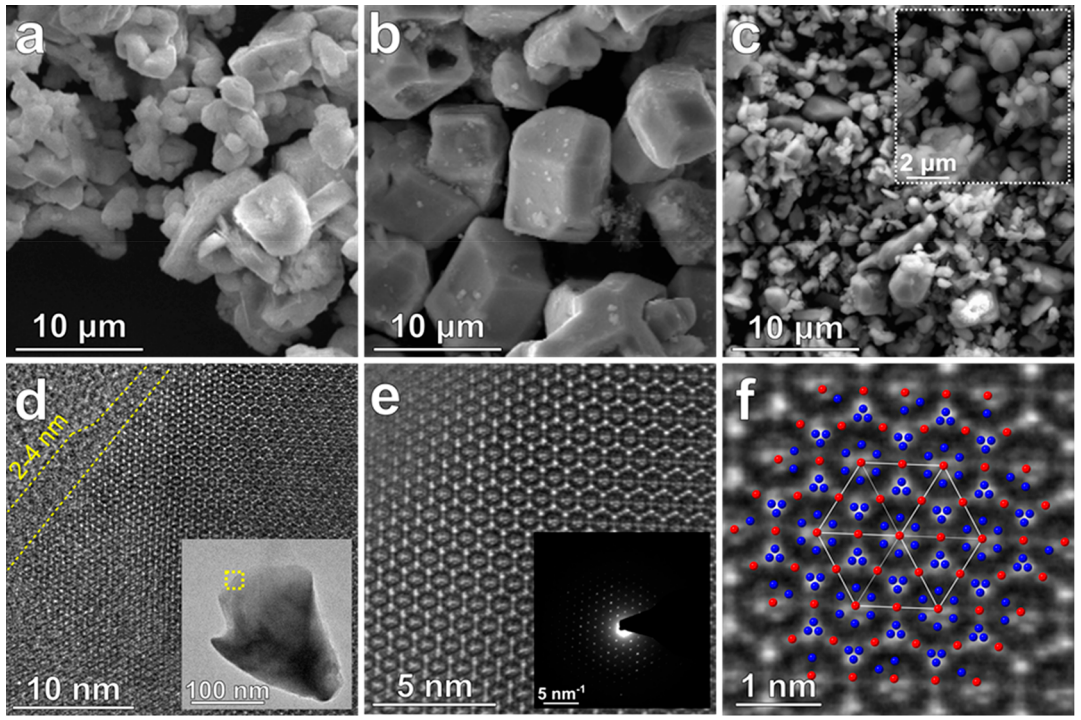

Figure 2. Representative SEM images of LLZTO powders synthesized by using MSS in the (a) chloride melt at 850 °C, (b) mixed melt at 700 °C, and (c) highly basic melt at 550 °C (higher magnification in the inset). TEM images of particle from highly basic melt: (d) phase contrast image of particle on carbon film with low-magnification image in the inset, with 2−4 nm surface Li_2CO_3 layer indicated by dashed yellow lines showing characteristic amorphous structure distinct from underlying holey carbon grid; (e) Wiener filtered phase contrast image of particle in (d) with nanoprobe electron diffraction pattern in the inset showing (111) crystal symmetry; and (f) zoom in of (e) with LLZTO (111) crystal structure overlaid with La (blue) and Zr/Ta (red) atoms shown generated by using CrystalMaker software based on structure from Logéat et al.[11]

properties (e.g., chlorides vs oxosalts) of the melt and resultant particle size.

Although the presence of a substantial amount of LiOH seems to favor the formation of large particles in the mixed medium, the addition of $LiNO_3$ and Li_2O_2 seems to promote formation of small LLZTO particles in the HB medium despite the large amount of LiOH in the melt. In addition, the HB melt can be seen to slowly bubble at 550 °C, most likely due to the decomposition of Li_2O_2 and subsequent liberation of O_2 gas,[52] which may in turn provide a sort of innate mixing that helps to more uniformly nucleate particles of LLZTO and distribute dissolved species. This innate mixing likely complements the reagent feeding method used for HB-MSS where reagents are added to the preheated melt, which is known to result in a smaller particle size distribution under comparable synthesis conditions.[53] The small particle size produced by the HB-MSS method allows for facile high-resolution TEM (HRTEM) imaging. Figure 2d shows a HRTEM image of a LLZTO particle synthesized by using HB-MSS, with a lower magnification image shown in the inset. A layer 2−4 nm thick is observed on the particle surface, which is attributed to the surface Li_2CO_3 layer that forms when LLZO is exposed to an ambient atmosphere.[54] A higher magnification image (Wiener-filtered to improve clarity) is in Figure 2e, with a corresponding (111) electron diffraction pattern in the inset. Finally, Figure 2f shows a zoomed image of Figure 2e with the LLZTO (111) crystal structure overlaid. These results indicate that primary particles synthesized from the HB-MSS method are single crystals.

The formation pathway of LLZTO in each of these synthesis methods is depicted graphically in Scheme 2. The trend of increasing Lux−Flood basicity and reduced garnet formation temperature is clear in the progression from the chloride, mixed, and highly basic molten salt media. The formation of crystalline LLZTO at only 550 °C by using HB-MSS is particularly interesting and to our knowledge is the lowest formation temperature for this garnet material reported to date. By comparison, SSR for LLZTO generally requires at least a single calcination at 900 °C for 8 h, although the majority of examples use higher temperatures, longer reaction times, and/or even multiple reaction steps (see Table 1 for comparison of experimental conditions for LLZTO using various methods).

To further decrease the viscosity of the HB-MSS medium and promote a smaller particle size distribution, a modified version of the HB melt was also investigated (which we call mHB-MSS), wherein a higher ratio of $LiNO_3$ and LiOH to Li_2O_2 was used (as described in the Experimental Section) to reduce viscosity and allow better intermixing of reagents and diffusion of solutes. In this case, reactions were performed at 550 °C for 4, 8, and 24 h to understand the particle size evolution of LLZTO in this medium (XRD patterns shown in Figure S4 and SEM images in Figure S5). After 4 h of reaction, many ultrafine nuclei are observed along with some larger particles on the order of 1 μm in size. After 8 h, the particle sizes are generally slightly smaller than the conventional HB-MSS method (particle size distributions for LLZTO from HB and mHB-MSS are compared in Figure S6) but less agglomerated, indicating that the mHB-MSS method improves mixing and particle dispersity despite the much longer reaction time, which is attributable to the lower viscosity of the mHB melt. Even for a reaction time of 24 h, the particle sizes do not

https://dx.doi.org/10.1021/acsaem.0c00716
ACS Appl. Energy Mater. 2020, 3, 6466−6475

Scheme 2. Depiction of Products Formed at Different Reaction Temperatures for Undoped LLZO and LLZTO Synthesized by Using Chloride (LiCl−KCl), Mixed (LiCl−LiOH), and Highly Basic ($LiNO_3$−LiOH−Li_2O_2) MSS Methods[a]

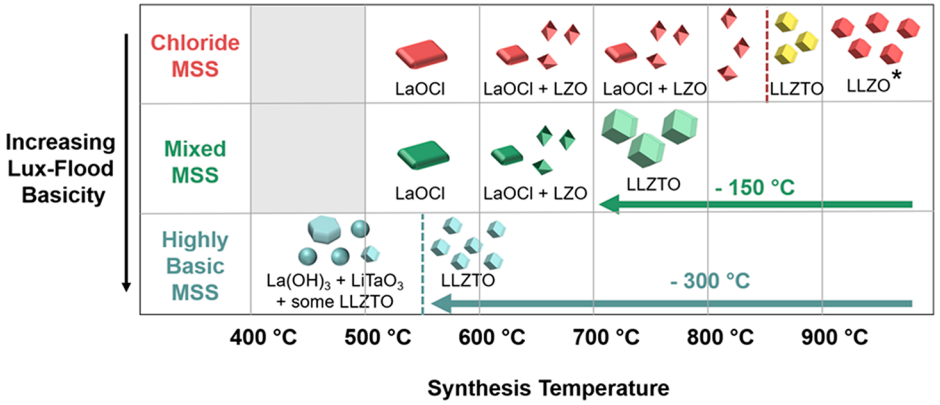

[a]Asterisk indicates results described in ref 35. Note the trend of decreased garnet formation temperature as the Lux−Flood basicity of the salt medium increases.

Table 1. Comparison of Properties of the LLZO Prepared Using Molten Salt Synthesis[a]

		synthesis conditions		sintering conditions		pellet properties			
molten salt medium	type of LLZO	temp (°C)	time (h)	temp (°C)	time (h)	relative density (%)	σ_{bulk}	σ_{tot}	ref
highly basic	LLZTO	550	2.5	1200	3	93.4	0.38	0.35	this work
modified highly basic	LLZTO	550	8	1200	4	91.1	0.73	0.61	this work
mixed	LLZTO	900	4	1200	2	78.5	NM	0.45^{G}	this work
chloride	LLZTO	900	4	1200	4	87.9	0.61	0.46	this work
chloride	ALLZO	900	4	1100	18	84	NM	0.23^{Au}	ref 35
chloride	GLLZO	900	4	1100	6	84	NM	0.37^{Au}	ref 35

[a]The bulk (where measurable using Sn−Li electrodes, σ_{bulk}) and total ionic conductivity (σ_{tot}) were measured at 25 °C and have units mS cm^{-1} (LLZTO = $Li_{6.4}La_3Zr_{1.4}Ta_{0.6}O_{12}$, ALLZO = $Al_{0.24}Li_{6.28}La_3Zr_2O_{12}$, and GLLZO = $Ga_{0.25}Li_{6.25}La_3Zr_2O_{12}$, NM = not measured; G: σ_{tot} measured using graphite electrodes; Au: σ_{tot} measured using sputtered gold electrodes.

increase substantially, but rather agglomeration of the primary particles increases. Finally, the improved melt properties of the mHB-MSS approach allow a lower ratio of salts to reagents of only 1.7:1 (compared to 5:1 for the HB-MSS method) by mass, substantially reducing waste.

3b. Ionic Conductivity of LLZTO Synthesized from Various MSS Methods. The LLZTO powders prepared from the different MSS methods were sintered at 1200 °C for various times to identify the optimized conditions, which are shown in Table 2. The relative density of the pellet sintered from LLZTO powder prepared from the chloride melt was roughly 88%, which is similar to our previous results for Al- and Ga-doped LLZO synthesized by using MSS in the same melt.[35] Before sintering, the LLZTO from the chloride and mixed MSS syntheses were ball-milled to improve sinterability while the as-synthesized powders from HB-MSS were already highly sinterable due to the smaller particle sizes. The density and ionic conductivity of mHB-MSS LLZTO were largely unaffected by ball-milling (see Figure S7a,b and Table S1). The relative density of the pellets from the mixed MSS was substantially lower (78.5%) while those for the HB methods were much higher (93.4% for HB and 91.1% for ball-milled mHB). It is not clear why powders synthesized by using the chloride and mixed MSS had low pellet densities, as after ball-milling the particle size distribution was comparable to that seen in the as-synthesized LLZTO particles from HB-MSS. We hypothesize that the postsynthesis washing step with water may have introduced a larger degree of proton exchange, which is known to have a deleterious effect on sinterability[35,55] for LLZTO synthesized in chloride and mixed MSS. The large starting particle sizes of the LLZTO from the mixed melts may also have a negative effect on sinterability even after ball-milling.

The room temperature bulk and total ionic conductivity and activation energies for lithium conduction of selected LLZTO samples from each of these MSS methods were determined (Supporting Information, Tables S1 and S2 show parameters used to calculate density and ionic conductivity). Because of the poor sinterability of the pellet from the mixed-MSS, only the total ionic conductivity was assessed (Figure S7c, fracture surface image shown in Figure S7d). Impedance spectra used for determining room temperature ionic conductivity of the LLZTO from HB, mHB, and chloride-MSS are plotted in Figure 3a with the characteristic frequencies of notable spectral features shown. Contributions from the bulk and grain boundary impedances along with calculated spectra from circuit fitting of these spectra are shown in Figure S8. From the results shown in Table 1, it is clear that the LLZTO from mHB-MSS displayed the highest total and bulk ionic conductivities from the MSS methods studied. An Arrhenius plot derived from the temperature dependence of ionic conductivity for HB, mHB, and chloride-MSS is shown in Figure 3b, with impedance spectra measured at various temperatures shown in Figure S9. In all three cases, the activation energies are between approximately 0.39 and 0.4 eV $atom^{-1}$, corresponding well with values reported in the literature (Table 2). The differences in ionic conductivity between the HB, mHB, and chloride-MSS samples can be

https://dx.doi.org/10.1021/acsaem.0c00716
ACS Appl. Energy Mater. 2020, 3, 6466−6475

Table 2. Properties of the Ta-Doped LLZO Prepared by MSS Herein Compared with Relevant Literature Results ($Li_{7-x}La_3Zr_{2-x}Ta_xO_{12}$, Where x = 0.6 Unless Otherwise Noted and Total Ionic Conductivity (σ_{tot}) Measured at 25 °C Unless Otherwise Noted)

	synthesis conditions		sintering conditions		pellet properties			
synthesis method	temp (°C)	time (h)	temp (°C)	time (h)	relative density (%)	σ_{tot} (mS cm^{-1})	E_a (eV)	ref
HB-MSS	550	2.5	1200	3	93.4	0.35	0.390	this work
modified HB-MSS	550	8	1200	4	91.1	0.61	0.402	this work
mixed MSS	900	4	1200	2	78.5	0.47		this work
chloride MSS[h]	900	4	1200	4	87.9	0.46	0.396	this work
SSR[i]	900	2 × 10	1130	36	94.1	0.28[d]	NR	ref 56
SSR[i]	900	2 × 10	1100	36	92.5	0.63[f]	0.36	ref 56
SSR[h,i]	950	2 × 6	1250	6	93.9	0.42	0.43	ref 57
SSR[h,i]	950	2 × 6	1280/1180	0.33/5	97	0.74	0.42−0.45	ref 47
SSR[h]	900	12	1180	12	91	0.33	0.53	ref 58
SSR	900	6	1200	24	84	0.15[a]	0.40	ref 59
SSR[i]	1× at 850/2× at 1000	3 × 20	1150	5	92.7	0.71[b,e]	0.42	ref 60
SSR[i]	900	NR[j]	1140	16	NR	1.0[b]	0.35	ref 41
coprecipitation	900	3−4	1050[g]	1	97.1	0.39[c]	0.45	ref 10
coprecipitation	900	3−4	1050[g]	1	97.8	0.82[d]	0.43	ref 10
solution-combustion synthesis	750	8	1125	6	NR	0.2	NR	ref 61
sol−gel	950	4	1100	4	89	0.14−0.21[d]	NR	ref 62
sol−gel	900	2	1000[g]	0.33	88	0.05	0.43	ref 25
polymer combustion	700	4	1100	12	93.6	0.67	0.42	ref 26
FZ single crystal growth	850	60	FZ[k]	FZ	100	∼1.0	0.39−0.47	ref 63

[a] σ_{tot} measured at 33 °C. [b] Al_2O_3 added as sintering aid. [c] x = 0.75. [d] x = 0.5. [e] x = 0.4. [f] x = 0.3. [g] Consolidated via hot-pressing. [h] High-energy ball milling (e.g., planetary milling, attrition milling, etc.) of LLZTO to reduce particle size. [i] Repeated grinding and heating steps (e.g., 2 × 10 = 2 calcination steps each for 10 h). [j] NR = not reported. [k] FZ = grown by floating zone single crystal growth method, sintering not applicable.

explained by a combination of grain boundary impedance (see Table S2) and difference in pre-exponential factor (mostly likely charge carrier concentration, which is known[10] to dominate in LLZO) since their activation energies are nearly identical.

LLZTO pellets consolidated from HB and mHB MSS powder seem to be highly sinterable based on the high pellet densities (Table 1). Fracture surface images of HB, mHB, and chloride-MSS pellets are shown in Figure 4. In all cases, a dense microstructure and a large degree of transgranular fracture is observed, indicating good grain cohesion despite the somewhat lower pellet density for the chloride-MSS LLZTO. Inspection of Figure 4 shows that the grain size (where it can be reasonably estimated from well-separated grains) appears to range between 2 and 10 μm, with some larger grains present, indicating substantial grain coarsening.

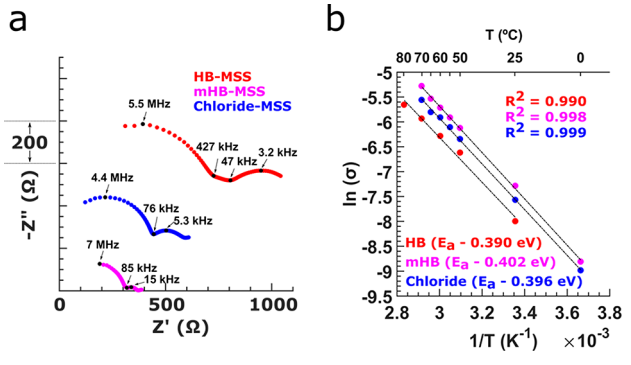

Figure 3. (a) Room temperature Nyquist plots (7 MHz−1 Hz) obtained using Sn−Li alloy electrodes for HB-MSS, mHB-MSS, and chloride-MSS pellets, with frequencies of pertinent features indicated (note: spectra are offset, −Z″ axis scale of 200 Ω between each major tick). (b) Arrhenius plot of ln(σ) (S cm^{-1}) vs T^{-1} (K^{-1}) for the same LLZTO pellets in (a) used to determine activation energy; fit quality (R^2) and calculated E_a (eV atom $^{-1}$) values are shown (see Figure S9 for EIS spectra used to determine temperature dependence of ionic conductivity for each sample).

The improved sinterability of the HB and mHB-MSS materials compared to the other MSS media may result from less severe proton exchange due to the high basicity of the salt medium used in the synthesis, producing an alkaline aqueous solution during washing, which has been shown to substantially reverse proton exchange.[64] However, the HB-MSS LLZTO has noticeably lower total ionic conductivity (0.35 mS cm^{-1}) than mHB-MSS LLZTO, comparable to that observed in the chloride and mixed melts, despite the much higher pellet densities. Further analysis of an HB-MSS pellet (sintered at 1300 °C to achieve a density higher than 95%) was performed by using backscatter electron (BSE) imaging and EDS of the pellet fracture surface (Figure S10). The BSE images reveal regions of substantially different contrast, and EDS spectra reveal high Ta content in the brighter grains, indicating the presence of elemental inhomogeneity in the pellet despite the high sintering temperature. For comparison, BSE images of the mHB and chloride-MSS pellets (Figure S10) do not display noticeable contrast differences, indicating more uniform composition between grains. We believe the lower ionic conductivity of the HB-MSS LLZTO may be related to this elemental inhomogeneity in the final dense ceramic pellets, which may produce nonoptimal lithium conduction in a large subset of the grains in the dense ceramic. To date, only Thompson et al. have observed elemental inhomogeneity in LLZTO with the aid of high-resolution synchrotron XRD.[10] The origins of elemental inhomogeneity in LLZTO from MSS and how to mitigate it are the focus of a larger subsequent

https://dx.doi.org/10.1021/acsaem.0c00716
ACS Appl. Energy Mater. 2020, 3, 6466−6475

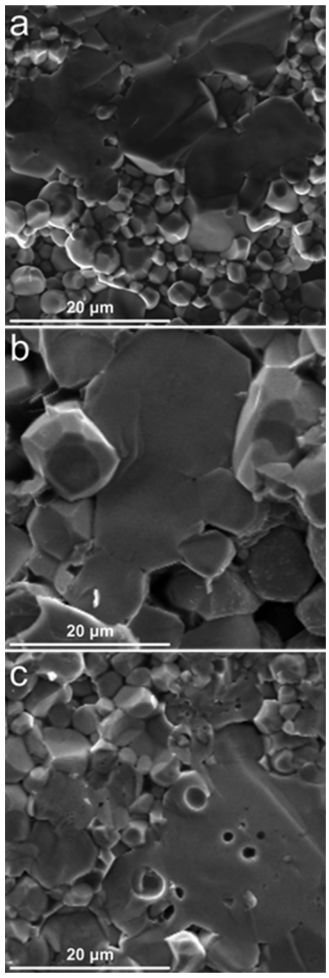

Figure 4. SEM fracture surface images of (a) an HB-MSS pellet), (b) an mHB-MSS pellet, and (c) a chloride-MSS pellet.

study and will be reported in a future publication. However, despite its presence and apparent effect on Li-ion conduction, the ionic conductivity of the HB LLZTO described herein still compares favorably with much of the literature (see Table 2) and indicates that reasonably good performance can be attained with a synthesis temperature that is drastically lower than those in conventional synthesis methods. More importantly, the mHB-MSS method utilizing a lower fraction of Li_2O_2 in the salt melt can produce sintered LLZTO pellets with higher ionic conductivity (0.61 mS cm^{-1}), indicating that this novel MSS method using a high Lux–Flood basicity medium enables formation of LLZTO at only 550 °C, with high ionic conductivity and relative density. Finally, the lower ratio of salts to reagents indicates that the mHB-MSS method may be comparably scalable to SSR despite the increased complexity due to the benefit of the substantially reduced synthesis temperature.

4. CONCLUSION

In conclusion, Ta-doped LLZO (LLZTO) of nominal composition $Li_{6.4}La_3Zr_{1.4}Ta_{0.6}O_{12}$ is obtained via molten salt synthesis (MSS) by using several different salt media with different Lux–Flood basicity. By use of a highly basic melt containing $LiNO_3$, LiOH, and Li_2O_2, the formation temperature of LLZTO decreases to only 550 °C; to our knowledge this is the lowest synthesis temperature for crystalline LLZTO reported to date, yielding a novel route toward synthesis temperatures that are considerably lower than conventional solid-state reactions (SSR) or other lower temperature synthetic routes such as sol–gel or combustion. In addition, by tuning the solution properties of the highly basic melt, small particle sizes and a low degrees of agglomeration are obtained by using synthesis at 550 °C for 8 h, which upon sintering at 1200 °C for 4 h results in pellets with relative density of 91.1% and a high bulk and total ionic conductivity of 0.73 and 0.61 mS cm^{-1}, respectively. Finally, the presence of elemental inhomogeneity within LLZTO pellets even after sintering at high temperatures is an interesting result that has implications for processing of garnets using Ta doping; this effect will be discussed in detail in a subsequent investigation.

■ ASSOCIATED CONTENT

Supporting Information

The Supporting Information is available free of charge at https://pubs.acs.org/doi/10.1021/acsaem.0c00716.

Procedures for EIS fitting, tabulated data, XRD patterns, SEM images, and EIS data (PDF)

■ AUTHOR INFORMATION

Corresponding Author

Candace K. Chan – *Materials Science and Engineering, School for Engineering of Matter, Transport and Energy, Arizona State University, Tempe, Arizona 85827, United States;* orcid.org/0000-0003-4329-4865; Email: candace.chan@asu.edu

Author

J. Mark Weller – *Materials Science and Engineering, School for Engineering of Matter, Transport and Energy, Arizona State University, Tempe, Arizona 85827, United States;* orcid.org/0000-0003-2056-8974

Complete contact information is available at: https://pubs.acs.org/10.1021/acsaem.0c00716

Notes

The authors declare no competing financial interest.

■ ACKNOWLEDGMENTS

This work was supported by the NSF CAREER Award DMR 1553519. J.M.W. acknowledges support from an ASU Fulton Schools of Engineering Dean's Fellowship. J.M.W. thanks Dr. Barnaby Levin for the Matlab code used for filtering TEM images. The authors gratefully acknowledge the use of facilities within the Eyring Materials Center at Arizona State University supported in part by NNCI-ECCS-1542160.

■ REFERENCES

(1) Knauth, P. Inorganic Solid Li Ion Conductors: An Overview. *Solid State Ionics* **2009**, *180* (14–16), 911–916.

(2) Thangadurai, V.; Narayanan, S.; Pinzaru, D. Garnet-Type Solid-State Fast Li Ion Conductors for Li Batteries: Critical Review. *Chem. Soc. Rev.* **2014**, *43* (13), 4714–4727.

(3) Albertus, P.; Babinec, S.; Litzelman, S.; Newman, A. Status and Challenges in Enabling the Lithium Metal Electrode for High-Energy and Low-Cost Rechargeable Batteries. *Nat. Energy* **2018**, *3* (1), 16–21.

(4) Murugan, R.; Thangadurai, V.; Weppner, W. Fast Lithium Ion Conduction in Garnet-Type $Li_7La_3Zr_2O_{12}$. *Angew. Chem., Int. Ed.* **2007**, *46* (41), 7778–7781.

(5) Zhang, Z.; Shao, Y.; Lotsch, B. V.; Hu, Y.-S.; Li, H.; Janek, J.; Nan, C.; Nazar, L.; Maier, J.; Armand, M.; Chen, L. New Horizons for Inorganic Solid State Ion Conductors. *Energy Environ. Sci.* **2018**, *11*, 1945−1976.
(6) Ramakumar, S.; Deviannapoorani, C.; Dhivya, L.; Shankar, L. S.; Murugan, R. Lithium Garnets: Synthesis, Structure, Li^+ Conductivity, Li^+ Dynamics and Applications. *Prog. Mater. Sci.* **2017**, *88*, 325−411.
(7) West, A. *Solid State Chemistry and Its Applications*, 2nd ed., Student Edition; Wiley: Chichester, West Sussex, UK, 2014.
(8) Rangasamy, E.; Wolfenstine, J.; Sakamoto, J. The Role of Al and Li Concentration on the Formation of Cubic Garnet Solid Electrolyte of Nominal Composition $Li_7La_3Zr_2O_{12}$. *Solid State Ionics* **2012**, *206*, 28−32.
(9) Wolfenstine, J.; Ratchford, J.; Rangasamy, E.; Sakamoto, J.; Allen, J. L. Synthesis and High Li-Ion Conductivity of Ga-Stabilized Cubic $Li_7La_3Zr_2O_{12}$. *Mater. Chem. Phys.* **2012**, *134* (2−3), 571−575.
(10) Thompson, T.; Sharafi, A.; Johannes, M. D.; Huq, A.; Allen, J. L.; Wolfenstine, J.; Sakamoto, J. A Tale of Two Sites: On Defining the Carrier Concentration in Garnet-Based Ionic Conductors for Advanced Li Batteries. *Adv. Energy Mater.* **2015**, *5*, 1500096.
(11) Logéat, A.; Köhler, T.; Eisele, U.; Stiaszny, B.; Harzer, A.; Tovar, M.; Senyshyn, A.; Ehrenberg, H.; Kozinsky, B. From Order to Disorder: The Structure of Lithium-Conducting Garnets $Li_{7-x}La_3Ta_xZr_{2-x}O_{12}$ (X = 0−2). *Solid State Ionics* **2012**, *206*, 33−38.
(12) Awaka, J.; Kijima, N.; Hayakawa, H.; Akimoto, J. Synthesis and Structure Analysis of Tetragonal $Li_7La_3Zr_2O_{12}$ with the Garnet-Related Type Structure. *J. Solid State Chem.* **2009**, *182* (8), 2046−2052.
(13) Yi, E.; Wang, W.; Kieffer, J.; Laine, R. M. Flame Made Nanoparticles Permit Processing of Dense, Flexible, Li^+ Conducting Ceramic Electrolyte Thin Films of Cubic-$Li_7La_3Zr_2O_{12}$ (c-LLZO). *J. Mater. Chem. A* **2016**, *4*, 12947−12954.
(14) Yi, E.; Wang, W.; Kieffer, J.; Laine, R. M. Key Parameters Governing the Densification of Cubic-$Li_7La_3Zr_2O_{12}$ Li^+ Conductors. *J. Power Sources* **2017**, *352*, 156−164.
(15) Fu, K.; Gong, Y.; Hitz, G. T.; McOwen, D. W.; Li, Y.; Xu, S.; Wen, Y.; Zhang, L.; Wang, C.; Pastel, G.; Dai, J.; Liu, B.; Xie, H.; Yao, Y.; Wachsman, E. D.; Hu, L. Three-Dimensional Bilayer Garnet Solid Electrolyte Based High Energy Density Lithium Metal−Sulfur Batteries. *Energy Environ. Sci.* **2017**, *10* (7), 1568−1575.
(16) Hitz, G. T.; Mcowen, D. W.; Zhang, L.; Ma, Z.; Fu, Z.; Wen, Y.; Gong, Y.; Dai, J.; Hamann, T. R.; Hu, L.; Wachsman, E. D. High-Rate Lithium Cycling in a Scalable Trilayer Li-Garnet-Electrolyte Architecture. *Mater. Today* **2019**, *22*, 50−57.
(17) Šepelák, V.; Bégin-Colin, S.; Le Caër, G. Transformations in Oxides Induced by High-Energy Ball-Milling. *Dalt. Trans.* **2012**, *41* (39), 11927−11948.
(18) Sakamoto, J.; Rangasamy, E.; Kim, H.; Kim, Y.; Wolfenstine, J. Synthesis of Nano-Scale Fast Ion Conducting Cubic $Li_7La_3Zr_2O_{12}$. *Nanotechnology* **2013**, *24* (42), 424005.
(19) Bitzer, M.; Van Gestel, T.; Uhlenbruck, S.; Hans-Peter-Buchkremer. Sol-Gel Synthesis of Thin Solid $Li_7La_3Zr_2O_{12}$ Electrolyte Films for Li-Ion Batteries. *Thin Solid Films* **2016**, *615*, 128−134.
(20) Shimonishi, Y.; Toda, A.; Zhang, T.; Hirano, A.; Imanishi, N.; Yamamoto, O.; Takeda, Y. Synthesis of Garnet-Type $Li_{7-x}La_3Zr_2O_{12-1/2x}$ and Its Stability in Aqueous Solutions. *Solid State Ionics* **2011**, *183* (1), 48−53.
(21) Janani, N.; Ramakumar, S.; Dhivya, L.; Deviannapoorani, C.; Saranya, K.; Murugan, R. Synthesis of Cubic $Li_7La_3Zr_2O_{12}$ by Modified Sol-Gel Process. *Ionics* **2011**, *17* (7), 575−580.
(22) Deviannapoorani, C.; Dhivya, L.; Ramakumar, S.; Murugan, R. Synthesis of Garnet Structured $Li_{7+x}La_3Y_xZr_{2-x}O_{12}$ (x = 0−0.4) by Modified Sol-Gel Method. *J. Sol-Gel Sci. Technol.* **2012**, *64* (2), 510−514.
(23) Afyon, S.; Krumeich, F.; Rupp, J. L. M. A Shortcut to Garnet-Type Fast Li-Ion Conductors for All-Solid State Batteries. *J. Mater. Chem. A* **2015**, *3* (36), 18636−18648.
(24) Gordon, Z. D.; Yang, T.; Morgado, G. B. G.; Chan, C. K. Preparation of Nano- and Microstructured Garnet $Li_7La_3Zr_2O_{12}$ Solid Electrolytes for Li-Ion Batteries via Cellulose Templating. *ACS Sustainable Chem. Eng.* **2016**, *4* (12), 6391−6398.
(25) El-Shinawi, H.; Cussen, E. J.; Corr, S. A. Enhancement of the Lithium Ion Conductivity of Ta-Doped $Li_7La_3Zr_2O_{12}$ by Incorporation of Calcium. *Dalton Trans.* **2017**, *46*, 9415−9419.
(26) Weller, J. M.; Whetten, J. A.; Chan, C. K. Non-Aqueous Polymer Combustion Synthesis of Cubic $Li_7La_3Zr_2O_{12}$ Nanopowders. *ACS Appl. Mater. Interfaces* **2020**, *12* (1), 953−962.
(27) Langer, F.; Glenneberg, J.; Bardenhagen, I.; Kun, R. Synthesis of Single Phase Cubic Al-Substituted $Li_7La_3Zr_2O_{12}$ by Solid State Lithiation of Mixed Hydroxides. *J. Alloys Compd.* **2015**, *645*, 64−69.
(28) Kim, K.; Yang, S. H.; Kim, M. Y.; Lee, M. S.; Lim, J.; Chang, D. R.; Kim, H. S. Cubic Phase Behavior and Lithium Ion Conductivity of $Li_7La_3Zr_2O_{12}$ Prepared by Co-Precipitation Synthesis for All-Solid Batteries. *J. Ind. Eng. Chem.* **2016**, *36*, 279−283.
(29) Yang, S. H.; Kim, M. Y.; Kim, D. H.; Jung, H. Y.; Ryu, H. M.; Han, J. H.; Lee, M. S.; Kim, H. S. Ionic Conductivity of Ga-Doped LLZO Prepared Using Couette−Taylor Reactor for All-Solid Lithium Batteries. *J. Ind. Eng. Chem.* **2017**, *56*, 422−427.
(30) Yang, T.; Gordon, Z. D.; Li, Y.; Chan, C. K. Nanostructured Garnet-Type Solid Electrolytes for Lithium Batteries: Electrospinning Synthesis of $Li_7La_3Zr_2O_{12}$ Nanowires and Particle Size-Dependent Phase Transformation. *J. Phys. Chem. C* **2015**, *119* (27), 14947−14953.
(31) Rosenthal, T.; Weller, J. M.; Chan, C. K. Needleless Electrospinning for High Throughput Production of $Li_7La_3Zr_2O_{12}$ Solid Electrolyte Nanofibers. *Ind. Eng. Chem. Res.* **2019**, *58* (37), 17399−17405.
(32) Fu, K.; Gong, Y.; Dai, J.; Gong, A.; Han, X.; Yao, Y.; Wang, C.; Wang, Y.; Chen, Y.; Yan, C.; Li, Y.; Wachsman, E. D.; Hu, L. Flexible, Solid-State, Ion-Conducting Membrane with 3D Garnet Nanofiber Networks for Lithium Batteries. *Proc. Natl. Acad. Sci. U. S. A.* **2016**, *113* (26), 7094−7099.
(33) Liu, X.; Fechler, N.; Antonietti, M. Salt Melt Synthesis of Ceramics, Semiconductors and Carbon Nanostructures. *Chem. Soc. Rev.* **2013**, *42* (21), 8237.
(34) Kimura, T. Molten Salt Synthesis of Ceramic Powders. In *Advances in Ceramics - Synthesis and Characterizatrion, Processing and Specific Applications*; Sikalidis, C., Ed.; InTech: 2011; pp 76−100.
(35) Weller, J. M.; Whetten, J. A.; Chan, C. K. Synthesis of Fine Cubic $Li_7La_3Zr_2O_{12}$ Powders in Molten LiCl-KCl Eutectic and Facile Densification by Reversal of Li^+/H^+ Exchange. *ACS Appl. Energy Mater.* **2018**, *1* (2), 552−560.
(36) Lux, H. Säuren" Und "Basen" Im Schmelzfluss: Die Bestimmung Der Sauerstoffionen-Konzentration. *Z. Elektrochem.* **1939**, *45*, 303.
(37) Flood, H.; Förland, T.; et al. The Acidic and Basic Properties of Oxides. *Acta Chem. Scand.* **1947**, *1*, 592−604.
(38) Guo, Q.; Wang, Q.; Chen, G.; Xu, H.; Wu, J.; Li, B. Molten Salt Synthesis of Transition Metal Oxides Doped $Li_4Ti_5O_{12}$ as Anode Material of Li-Ion Battery. *ECS Trans.* **2016**, *72* (9), 11−23.
(39) Rahman, M. M.; Wang, J. Z.; Hassan, M. F.; Chou, S.; Wexler, D.; Liu, H. K. Basic Molten Salt Process-A New Route for Synthesis of Nanocrystalline $Li_4Ti_5O_{12}$-TiO_2 Anode Material for Li-Ion Batteries Using Eutectic Mixture of $LiNO_3$-LiOH-Li_2O_2. *J. Power Sources* **2010**, *195* (13), 4297−4303.
(40) Du, Y.; Inman, D. Preparation of Zirconia Powders from Molten Nitrites and Nitrates. *J. Mater. Sci.* **1996**, *31*, 5505−5511.
(41) Li, Y.; Han, J. T.; Wang, C. A.; Xie, H.; Goodenough, J. B. Optimizing Li^+ Conductivity in a Garnet Framework. *J. Mater. Chem.* **2012**, *22* (30), 15357−15361.
(42) Allen, J. L.; Wolfenstine, J.; Rangasamy, E.; Sakamoto, J. Effect of Substitution (Ta, Al, Ga) on the Conductivity of $Li_7La_3Zr_2O_{12}$. *J. Power Sources* **2012**, *206*, 315−319.
(43) Kim, Y.; Yoo, A.; Schmidt, R.; Sharafi, A.; Lee, H.; Wolfenstine, J.; Sakamoto, J. Electrochemical Stability of $Li_{6.5}La_3Zr_{1.5}M_{0.5}O_{12}$ (M = Nb or Ta) against Metallic Lithium. *Front. Energy Res.* **2016**, *20*, 1−7.
(44) Patnaik, P. *Handbook of Inorganic Chemicals*; McGraw-Hill: New York, NY, 2003.

https://dx.doi.org/10.1021/acsaem.0c00716
ACS Appl. Energy Mater. 2020, 3, 6466−6475

(45) Huang, X.; Lu, Y.; Guo, H.; Song, Z.; Xiu, T.; Badding, M. E.; Wen, Z. None-Mother-Powder Method to Prepare Dense Li-Garnet Solid Electrolytes with High Critical Current Density. *ACS Appl. Energy Mater.* **2018**, *1* (10), 5355−5365.
(46) Huang, X.; Lu, Y.; Song, Z.; Rui, K.; Wang, Q.; Xiu, T.; Badding, M. E.; Wen, Z. Manipulating Li_2O Atmosphere for Sintering Dense $Li_7La_3Zr_2O_{12}$ Solid Electrolyte. *Energy Storage Mater.* **2019**, *22*, 207−217.
(47) Huang, X.; Xiu, T.; Badding, M. E.; Wen, Z. Two-Step Sintering Strategy to Prepare Dense Li-Garnet Electrolyte Ceramics with High Li^+conductivity. *Ceram. Int.* **2018**, *44* (5), 5660−5667.
(48) Shao, Y.; Wang, H.; Gong, Z.; Wang, D.; Zheng, B.; Zhu, J.; Lu, Y.; Hu, Y.-S.; Guo, X.; Li, H.; Huang, X.; Yang, Y.; Nan, C.-W.; Chen, L. Drawing a Soft Interface : An Effective Interfacial Modification Strategy for Garnet-Type Solid-State Li Batteries. *ACS Energy Lett.* **2018**, *3*, 1212−1218.
(49) Wang, C.; Xie, H.; Zhang, L.; Gong, Y.; Pastel, G.; Dai, J.; Liu, B.; Wachsman, E. D.; Hu, L. Universal Soldering of Lithium and Sodium Alloys on Various Substrates for Batteries. *Adv. Energy Mater.* **2018**, *8*, 1701963.
(50) Miara, L. J.; Ong, S. P.; Mo, Y.; Richards, W. D.; Park, Y.; Lee, J. M.; Lee, H. S.; Ceder, G. Effect of Rb and Ta Doping on the Ionic Conductivity and Stability of the Garnet $Li_{7+2x-y}(La_{3-x}Rb_x)(Zr_{2-y}Ta_y)O_{12}$ ($0 \le x \le 0.375$, $0 \le y \le 1$) Superionic Conductor: A First Principles Investigation. *Chem. Mater.* **2013**, *25* (15), 3048−3055.
(51) Claes, P.; Peeters, G.; Glibert, J. Chemical and Electrochemical Behavior in Molten Alkali Hydroxides: III. Chemistry of Tin (II) and (IV) in the NaOH-KOH Eutectic Mixture and in Pure NaOH. *J. Electrochem. Soc.* **1989**, *136* (9), 2599−2603.
(52) Yao, K. P. C.; Kwabi, D. G.; Quinlan, R. A.; Mansour, A. N.; Grimaud, A.; Lee, Y.; Lu, Y.; Shao-horn, Y. Thermal Stability of Li_2O_2 and Li $_2$ O for Li-Air Batteries: In Situ XRD and XPS Studies. *J. Electrochem. Soc.* **2013**, *160* (6), 824−831.
(53) Vradman, L.; Friedland, E.; Zana, J.; Vidruk-Nehemya, R.; Herskowitz, M. Molten Salt Synthesis of $LaCoO_3$ Perovskite. *J. Mater. Sci.* **2017**, *52* (19), 11383−11390.
(54) Cheng, L.; Liu, M.; Mehta, A.; Xin, H. L.; Lin, F.; Persson, K. A.; Chen, G.; Crumlin, E. J.; Doeff, M. M. Garnet Electrolyte Surface Degradation and Recovery. *ACS Appl. Energy Mater.* **2018**, *1*, 7244−7252.
(55) Reddy, M. V.; Adams, S. Molten Salt Synthesis and Characterization of Fast Ion Conductor $Li_{6.75}La_3Zr_{1.75}Ta_{0.25}O_{12}$. *J. Solid State Electrochem.* **2017**, *21*, 2921−2928.
(56) Wang, Y.; Lai, W. High Ionic Conductivity Lithium Garnet Oxides of $Li_{7-x}La_3Zr_{2-x}Ta_xO_{12}$ Compositions. *Electrochem. Solid-State Lett.* **2012**, *15* (5), A68−A71.
(57) Huang, X.; Lu, Y.; Jin, J.; Gu, S.; Xiu, T.; Song, Z.; Badding, M. E.; Wen, Z. Method Using Water-Based Solvent to Prepare $Li_7La_3Zr_2O_{12}$ Solid Electrolytes. *ACS Appl. Mater. Interfaces* **2018**, *10* (20), 17147−17155.
(58) Yi, M.; Liu, T.; Wang, X.; Li, J.; Wang, C.; Mo, Y. High Densification and Li-Ion Conductivity of Al-Free $Li_{7-x}La_3Zr_{2-x}T_axO_{12}$ Garnet Solid Electrolyte Prepared by Using Ultrafine Powders. *Ceram. Int.* **2019**, *45* (1), 786−792.
(59) Janani, N.; Ramakumar, S.; Kannan, S.; Murugan, R. Optimization of Lithium Content and Sintering Aid for Maximized Li^+ Conductivity and Density in Ta-Doped $Li_7La_3Zr_2O_{12}$. *J. Am. Ceram. Soc.* **2015**, *98* (7), 2039−2046.
(60) Tsai, C. L.; Roddatis, V.; Chandran, C. V.; Ma, Q.; Uhlenbruck, S.; Bram, M.; Heitjans, P.; Guillon, O. $Li_7La_3Zr_2O_{12}$ Interface Modification for Li Dendrite Prevention. *ACS Appl. Mater. Interfaces* **2016**, *8*, 10617.
(61) Chen, X.; Cao, T.; Xue, M.; Lv, H.; Li, B.; Zhang, C. Improved Room Temperature Ionic Conductivity of Ta and Ca Doped $Li_7La_3Zr_2O_{12}$ via a Modified Solution Method. *Solid State Ionics* **2018**, *314*, 92−97.
(62) Yoon, S. A.; Oh, N. R.; Yoo, A. R.; Lee, H. G.; Lee, H. C. Preparation and Characterization of Ta-Substituted $Li_7La_3Zr_{2-x}O_{12}$ Garnet Solid Electrolyte by Sol-Gel Processing. *Han'guk Seramik Hakhoechi* **2017**, *54* (4), 278−284.
(63) Kataoka, K.; Akimoto, J. Lithium-Ion Conductivity and Crystal Structure of Garnet-Type Solid Electrolyte $Li_{7-x}La_3Zr_{2-x}Ta_xO_{12}$ Using Single-Crystal. *J. Ceram. Soc. Jpn.* **2019**, *127* (8), 521−526.
(64) Ma, C.; Rangasamy, E.; Liang, C.; Sakamoto, J.; More, K. L.; Chi, M. Excellent Stability of a Lithium-Ion-Conducting Solid Electrolyte upon Reversible Li^+/H^+ Exchange in Aqueous Solutions. *Angew. Chem., Int. Ed.* **2015**, *54* (1), 129−133.

https://dx.doi.org/10.1021/acsaem.0c00716
ACS Appl. Energy Mater. 2020, 3, 6466−6475